JJEES

Jordan Journal of Earth and Environmental Sciences

JJEES (2022) 13 (4): 247-262
ISSN 1995-6681

Landsat / MODIS Fusion for Soil Moisture Estimation Over a Heterogeneous Area in Northern Jordan

Ali Almagbile[1,2*], Khaled Hazeymeh[1,2], Mostafa Mosleh[3], Abdulla Al-Rawabdeh[4,2], Omar Aldayafleh[1], Mohammad Zeitoun[1], Amer Maslamani[1]

[1]*Department of Geography, Yarmouk University, 21163 Irbid, Jordan*
[2]*Applied Geoinformatics Laboratory, Yarmouk University, 21163 Irbid, Jordan*
[3]*Department of Geography, Faculty of Arts, South Valley University, Qena 83523, Egypt*
[4]*Department of Earth and Environmental Sciences, Yarmouk University, 21163 Irbid, Jordan*

Received 17th October 2021; Accepted 9th April 2022

Abstract

Fusion models have been developed to improve the spatial and temporal resolution simultaneously because remote sensing data cannot guarantee the high resolution of vegetation and temperature products. In this study, Moderate Resolution Imaging Spectroradiometer (MODIS) and Land Remote Sensing Satellite (Landsat) data were fused using the STI-FM fusion model for retrieving soil moisture index (SMI) based on the NDVI-LST triangulation/trapezoidal shape. The study was conducted from November 2019 to May 2020 and covered a heterogeneous area in Northern Jordan. For validation, the soil moisture index results were then compared with the observed in-situ soil moisture measurements at 16 sites distributed throughout the study area. To determine the spatial and temporal variability/stability of SMI and observed soil moisture, statistical and geostatistical approaches were employed. The results revealed that the relationship between SMI and in-situ measurements was high in the wet winter months and low during the warm summer months. The determination coefficient r^2 of 0.66 and RMSE of 0.10 were found in January while in May, the r^2 and RMSE were 0.35 and 0.32, respectively. The results of the semi-variogram analysis showed that the observed soil moisture was more varied during the wet periods when compared with the drier period, whereas the SMI was not influenced by seasonal variations. The results indicated that high values of SMI can be obtained with low temperature and rich vegetation, while the higher temperature and water-stressed vegetation revealed low SMI values.

Keywords: *Soil moisture index, Data fusion, NDVI-LST space, Land surface temperature, NDVI, In-situ measurements*

1. Introduction

One of the key components for understanding soil moisture variability in spatial and temporal scales involves analyzing the inter-relationship between vegetation and temperature indices. The variation of soil properties, such as texture, porosity, permeability, and organic matter, could affect the distribution of soil moisture at local scales (Mohanty and Skaggs 2001). Topography in terms of slope, aspects, and curvature could also have a significant contribution to soil moisture variations even over a small area as they could determine the runoff and evapotranspiration rates. The Topographic Wetness Index (TWI) (Beven and Kirkby 1979) is common and widely used in determining the spatial variation of soil moisture and runoff generation (Grabs et al. 2009). Vegetation type and density might influence the spatiotemporal distribution of soil moisture as they control the infiltration, runoff generation, evapotranspiration rates, and the dynamic of soil water-retention capacity (Mohanty and Skaggs 2001, Jin et al. 2011). Since vegetation responds to precipitation, its influence on soil moisture variation is more dynamic in comparison with the topography factor.

Generally, soil moisture estimates can be extracted by either direct or indirect techniques (Dorigo et al. 2011, Almagbile et al. 2019). The direct technique involves a gravimetric method that calculates soil moisture as a percentage by weighting the moist soil, then oven drying it at 105 Celsius, and reweighting the dried soil. Whereas indirect methods measure soil moisture through electromagnetic instruments such as neutron probes, capacitance sensors, time-domain reflectometry (TDR), Tensiometers, electrical resistance blocks, and Psychrometers. The trade-off between these sensors varies in terms of sensor costs, the size of soil moisture data, and the wetness status of the soil (Bogena et al. 2007, Robinson et al. 2008, Seneviratne et al. 2010, Dorigo et al. 2011).

Although in-situ-based measuring of soil moisture could provide more reliable and accurate measurements of the actual amount of water in the soil at various depths, these measurements are limited in their spatial and temporal scales. To overcome this, remote sensing methods have been extensively used in mapping soil moisture variability at larger spatial extents (Xu et al. 2018). In this context, Soil Moisture Index (SMI) is widely applied. SMI is normally calculated by employing the universal triangular/trapezoidal eigenspace theories of the relationship between land surface temperature (LST) and normalized vegetation index (NDVI) (Carlson 2007, Choi and Hur 2012) using the optical and thermal spectral bands of different satellite systems such as

* Corresponding author e-mail: a.magbile@yu.edu.jo

Moderate Resolution Imaging Spectroradiometer (MODIS) and Landsat (Sandholt et al. 2002, Sun et al. 2012, Xu et al. 2018, Fan et al. 2019).

Since remote sensing observations have either a high spatial resolution or high temporal resolution, MODIS/Landsat fusion models have been developed to produce high-resolution data in both temporal and spatial scales. Such models include the Spatial and Temporal Adaptive Reflectance Fusion Model (STARFM) (Gao 2006), the Spatial-temporal Adaptive Data Fusion Algorithm for Temperature mapping (SADFAT) (Weng et al., 2014), and the Spatial-temporal Image Fusion Model (STI-FM) (Hazaymeh and Hassan 2015a).

The relationship between soil moisture and Normalized Difference Vegetation Index (NDVI) has been investigated intensively (e.g., Farrar et al. 1994, Liu and Kogan 1996, Adegoke and Carleton 2002, Wang et al. 2007, Schnur et al. 2010). These studies found that NDVI and soil moisture are significantly correlated. In recent years, fusion models have emerged for computing soil moisture index by analyzing the NDVI-LST relationship. The scope of these investigations was to emphasize the importance of improving the spatial and temporal resolution of soil moisture products for accurately enhancing many agricultural and agroclimatic applications such as agriculture monitoring, drought and flood analysis, and natural resource reservations. Zhong et al. (2018) adopted downscaling technique for soil moisture retrieving using microwave soil moisture products whereas Xu et al. (2018) employed a downscaling method based on MODIS/Landsat fusion algorithm for retrieving surface soil moisture. These studies used in-situ soil moisture measurements for validating remote sensing data.

Apart from estimating soil moisture from NDVI-LST relationship space, several previous studies (e.g., Hills and Reynolds 1969, Hawely et al. 1983, Westren et al. 1999, Mohanty et al. 2000, Mohanty and Skaggs 2001) have been conducted for analyzing soil moisture in heterogeneous environments. The relationship between soil moisture patterns and other environmental factors such as topography and vegetation has been intensively studied on different spatial and temporal scales. Early attempts were conducted by Hills and Reynolds (1969) to find a relationship between soil moisture and slope and found that no significant relationship existed. In a small agricultural watershed, however, Hawely et al. (1983) found that the variation of soil moisture was greatly affected by the topography factor. This result was also found by Mohanty et al (2000). Grabs et al. (2009) developed a new wetness index to show its capacity to truly predict the spatial distribution of soil moisture. Soil moisture dynamic concerning the land cover was also investigated. In complex terrain with mixed vegetation, Hawely et al. (1983) found that temporal soil moisture tends to be more stable in comparison with sparse vegetation.

To determine the relationship between moisture and environmental factors (temperature, topography, and vegetation), various statistical approaches were used. These approaches can be categorized into descriptive and analytical statistics such as mean, variation coefficient, standard deviation, correlation and regression, and geostatistical analysis (e.g., Qiu et al. 2001, Brocca et al. 2010). The influence of the environmental variables on soil moisture can be determined using intrinsic methods such as principal component analysis (Zhang and Oxley 1994). The extrinsic methods, on the other hand, are divided into linear (e.g., canonical correlation analysis) and nonlinear such as canonical correspondence analysis (Qiu et al. 2001). Although both linear and nonlinear methods are powerful in relating the soil moisture pattern to environmental factors, the nonlinear methods have been proven to be more robust than the linear methods (Zhang and Oxley 1994, Qiu et al. 2001). In a similar environment, Ibrahim et al (2021) evaluated the influences of LST on NDVI, SMI, normalized difference water index (NDWI), and dry bare soil index (DBSI) using a series of Landsat and MODIS images. The results showed that the SMI decreased by around 44 % in 2019 compared with those 1990. Using correlation analysis techniques, Jaber (2018) investigated the relationships between vegetation abundance and LST in different seasons in the years 1987 and 2016 in urban areas in Greater Amman Municipality. The results showed a negative relationship between vegetation abundance and LST in summer, while a positive relationship was found in winter. Jaber (2021) also demonstrated the relationship between NDVI and daytime and nighttime LST in Jordan based on MODIS data in different seasons in 2017. The results showed that the variability in NDVI can be explained by land cover. However, the variation in the daytime and nighttime LST can slightly be correlated to the variation in land cover.

The main objective of this study is to infer the spatial variation of soil moisture over a heterogeneous environment in northern Jordan based on integrated ground soil data and remote sensing data. To improve the spatial and temporal resolution of soil moisture products, remote sensing data including MODIS and Landsat-8 data are fused using the STI-FM technique (Hazaymeh and Hassan, 2015a, b). More specifically, this study aims to (i) investigate the relationship between the normalized difference vegetation index (NDVI) and land surface temperature (LST) using high spatiotemporal fused data (ii) estimate soil moisture at high spatial and temporal scales, (iii) validate the estimated remote sensed-based soil moisture with ground-based soil moisture, and (iii) demonstrate the variation of the observed and estimated soil moisture in both spatial and temporal dimensions.

2. Material and methods

2.1 Study area

The study area is in the northern part of Jordan (32° 23′ to 32° 28′ N and 35° 49′ and 36° 2′ E) with an approximate area of 50 km^2 (Figure 1). This study area was chosen because it has heterogeneous characteristics in terms of topography, climate, vegetation, and soil. Thus, soil moisture is subject to wide variations within a short distance and time. The characteristics of vegetation and soil type provided below were observed during our soil sampling campaigns which were conducted between November 2019 and May 2020.

Geographically, the study can be divided into three parts:

(1) The hillslope area is in the western part of the study area and has a topography that varies from complex to moderate relief with elevation ranges between 600m and 1150 m above mean sea level. The climate is characterized by hot-dry summer and modest wet winter. The annual averages of rainfall and temperature are 580 mm and 14.4 ^{o}C, respectively. These vegetation types are natural vegetation such as wild pistachios (Pistacia Atlantica), evergreen oak (Quercus ilex), pine (Pinus), Carbo tree (Ceratonia siliqua), and wild strawberry (Fragaria vesca) common, as well as cereal crops (e.g., Wheat (Triticum), barley (Hordeum vulgare), and lentil (Lens culinaris)) and orchards (Olives (Olea europaea), apple (Malus Domestica), nectarine (Prunus persica var. nucipersica), peach (Prunus persica), and vine (Vitis)), particularly in the moderately sloped areas. Soil types consist of fine and coarse textures with predominantly clay, silt, and loam.

(2) The gentle-sloped area is in the eastern part of the study area and has moderate relief with elevation ranges between 500 to 800 meters above mean sea level. The climate is a transition from sub-humid to semi-arid with annual averages of rainfall and temperature of 140 mm and 16.9 ^{o}C, respectively. In almost all months, the precipitation in this area is less than the evaporation. The vegetation and land cover include grass and pasture; thus, a huge part of this area is allocated for grazing. In the areas located close to the sub-humid climate, Wheat (Triticum), barley (Hordeum vulgare), and lentil (Lens culinaris) crops are cultivated. The soil type is a coarse and fine texture with sand and loam.

(3) The plain area is located between the abovementioned areas. It has moderate climate conditions with annual average precipitation and temperature of 460mm and 17.8 ^{o}C, respectively. It is characterized by simple topography with elevation ranges between 450 to 650 meters above sea mean level. Clay soil is predominant with small patches of silt and loam. Agricultural lands include orchards which consist mainly of Olives (Olea europaea), apples (Malus Domestica), nectarine (Prunus persica var. nucipersica), peach (Prunus persica), and vine (Vitis)), and the dominant crops including Wheat (Triticum), barley (Hordeum vulgare), and lentil (Lens culinaris) which occur in most parts of this part of the study area.

Figure 2 which shows the elevation and slope (degrees) in the study area, was derived from Aster Global Digital Elevation Model (DEM) with a 30-meter resolution (https://search.earthdata.nasa.gov/search). The percentage of variations of sand, clay, and silt was interpolated using ordinary kriging based on the observed soil data during our sampling campaign (Figure 3). As can be seen, the heterogeneity of the landscape features in the study area would in turn have a significant effect on the spatiotemporal variation of soil moisture.

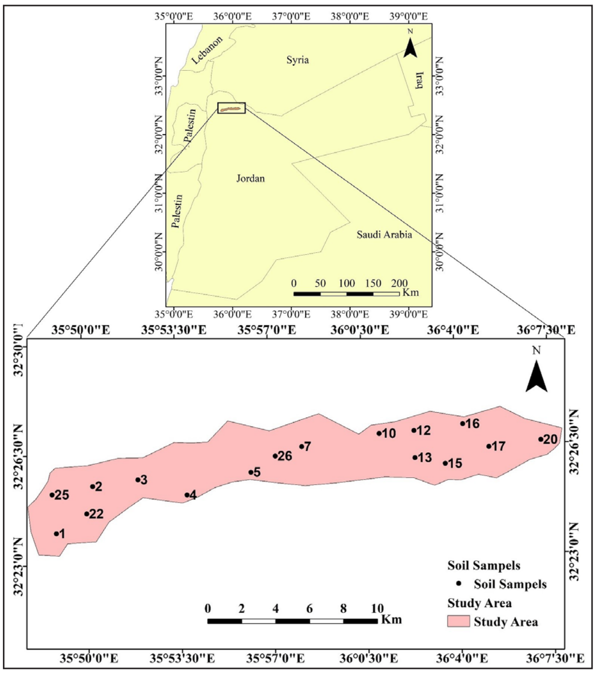

Figure 1. The geographic extent of Jordan (up) and the geographic extent of the study area with soil sample locations (bottom).

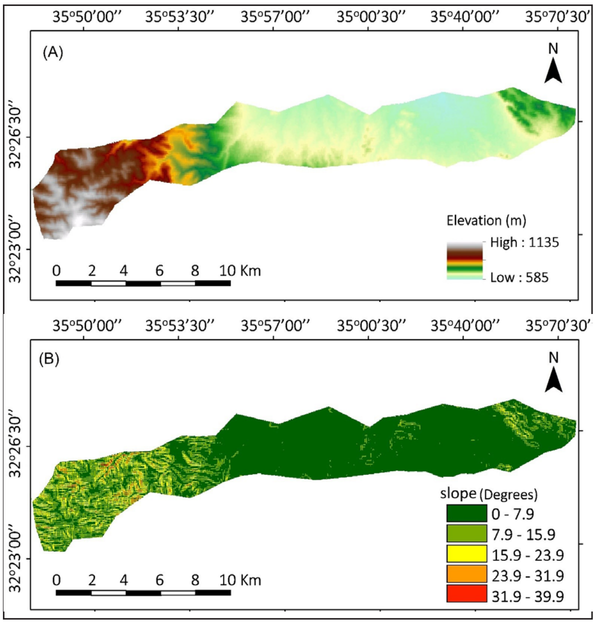

Figure 2. SRTM-30m digital elevation model (A), and the generated slope (B) of the study area

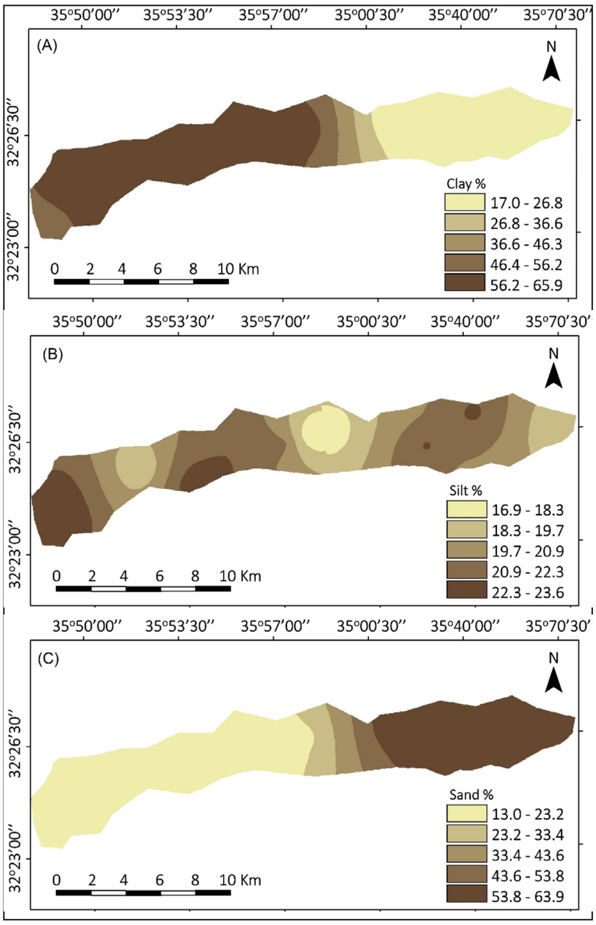

Figure 3. Soil texture characteristics based on soil textural triangle, percentage of clay (A), silt (B), and sand (C) in the study area

In Situ measurements

Soil data were collected from 16 sample locations spread over the study area (Figure 1) at depth of 10 cm. Table 1 shows the description of soil samples, soil moisture % and the soil type for each sample location. Field visits were conducted once a month from November 2019 to May 2020. The position of each soil sample was determined using a real-time kinematic (RTK) receiver with approximately 3cm level accuracy. It is worth mentioning that the following restrictions have been considered during soil samples collection:

- In the case of the hilly area, the samples were taken on a gentle slope and the steep slope was avoided because the soil depth is very shallow.
- during rainfall events, sampling was suspended.
- All soil samples were taken in rainfed areas, thus irrigated areas were avoided.
- The minimum distance between sample locations was at least 2 km to avoid homogeneity of topography, vegetation, and soil.
- To avoid human activities such as industrial, trading, and irrigated agriculture which may influence the soil, built-up areas (urban areas), road networks, and dense tree canopy were avoided.

After soil samples were collected, soil moisture was computed in the laboratory using the volumetric soil moisture method. In this method, each soil sample was weighed before and after oven drying. Then the water content in each sample was converted to a percentage value. The volumetric method was selected due to its simplicity, robustness, and low technical work required to derive the soil water content (Robock et al. 2000, Seneviratne et al. 2010). Therefore, it is widely used for calibrating indirect methods such as neutron probes (Almagbile et al. 2019).

Table 1. Description of the sixteen soil samples used to calculate the reference soil moisture measurements in this study

Sample	Location ID	X	Y	SM %	soil type	LULC
1	7	32.40123	35.81503	18.4	clay	Grass
2	26	32.42580	35.83848	16.6	clay	bare soil
3	16	32.42877	35.86696	19.3	clay	bare soil
4	10	32.42002	35.89748	16.5	clay	bare soil
5	12	32.43119	35.93785	17.7	clay	wheat crop
6	20	32.44408	35.97006	13.5	clay	bare soil
7	17	32.44988	36.01881	12.8	sand-loam	grass
8	13	32.45095	36.04061	12.2	sand-loam-clay	grass
9	15	32.43652	36.04082	13.9	sand-loam	grass
10	5	32.43306	36.05966	9.8	sand-loam-clay	grass
11	2	32.45389	36.07126	10.9	sand-loam	grass
12	3	32.44138	36.08727	9.5	sand-loam	grass
13	25	32.44432	36.11991	9.3	sand-loam	grass
14	4	32.41133	35.83432	19.1	clay	orchard
15	22	32.42196	35.81295	18.0	clay	orchard
16	1	32.43943	35.95331	15.2	clay	orchard

Remote Sensing Datasets

NDVI and LST

Table 2 illustrates the characteristics of the remote sensing dataset that has been used in this study. Two types of datasets were used (i) MODIS collections (i.e., MOD13Q1 and MOD11A2). The MOD13Q1 collection provides the composite NDVI values over 16 days at 250m spatial resolution where cloud-free global coverage is achieved by replacing clouds with the historical MODIS time series climatology record. The MOD11A2 provides composite 8-day LST data at 1km spatial resolution. The MOD11A2 collection comprised daytime and night-time LSTs, quality assurance assessment, observation times, view angles, bits of clear sky days and nights, and emissivity estimated using the spectral bands 31 and 32 concerning land cover types. (ii) The Landsat 8 Operation Land Imager (OLI) and Thermal Infrared Sensor (TIRS) at 30m spatial resolution. Here, the red (0.64-0.67 μm), near-infrared (0.85-0.88 μm), and thermal (10.6-11.19 μm) spectral bands were used to calculate the NDVI and LST maps.

Table 2. Characteristics of remote sensing dataset used in this study

Satellite	MODIS 8day composite		Landsat-8 (L8)	
Product	NDVI	LST	NDVI	LST
Collection	MOD13Q1	MOD11A2	Level 2	Level 2
Type	16-day composite	8-day composite	individual day	individual day
Spatial Resolution	250m	1000m	30m	30m
Spectral bands	Red and NIR	TIR 31 and 32	Red and NIR	TIR 10
MODIS Day of the Year, L8 Acquisition date	**2019**: 329, 337, 345, 353, 361 **2020**: 001, 009, 025, 033, 041, 0.49, 057, 065, 072, 081, 089, 097, 105, 129		2019/11/26, 2020/02/14, 2020/04/02, 2020/04/18, 2020/05/04, 2020/05/20	
Path/Raw	v05/h21		174/037	
Sources	Google Earth Engine			

Data processing

In this study, original NDVI and LST images were used to generate synthetic Landsat-like NDVI and LST by fusing the original MODIS and Landsat 8 using the STI-FM model. The fusion of MODIS and Landsat 8 allows the generation of synthetic images at the spatial resolution of Landsat 8 (i.e., 30m) and the temporal resolution of the MODIS product. From the relationship between the LST and NDVI, the soil moisture index is retrieved.

Calculating NDVI and LST using a data fusion model

STI-FM is a recently developed model that used two MODIS images taken at time one and time two, and one Landsat image taken at the time one [$L_{(t1)}$] to generate a synthetic Landsat surface reflectance and land surface temperature image at time two. The STI-FM model begins with determining the rate of the temporal change in spectral signatures between the two MODIS images at times one and two. Based on this relationship, the temporal changes might be either positive or negative change. In some cases, however, no change could be identified. In the second step, a linear relationship between the MODIS images for each case of change is developed (Hazaymeh and Almagbile 2018). Finally, a synthetic Landsat surface reflectance or surface temperature image at time two $synth\_L(t_2)$ is generated using the regression coefficients computed in the second step as follows:

$$synth_{L(t_2)} = a * L_{(t1)} + c \quad \text{(1)}$$

where a and c are the slope and intercept, respectively. Note that STI-FM has been validated in previous work and used in developing a remote sensing-based agricultural drought indicator and successfully implemented over a semi-arid region in Jordan.

Soil Moisture Index

Early studies (Carlson 1986, Gillies, and Carlson 1995) used the vegetation index/temperature (VIT) trapezoidal shape for determining soil moisture index (Figure 4).

The trapezoidal shape in the Ts-VIs scatters plots emerge due to the negative relationship between these two variables. For instance, Ts have low sensitivity to the variation of water content over vegetated areas, while it has high sensitivity over bare soils. For example, a non-water stress condition can be identified when the VIs values increase along the x-axis while the Ts values decrease along the *y*-axis. This is due to the cooling effects of evapotranspiration, and vice versa. In the Ts-VIs scatter plot, the VIs and Ts are represented on the *x*-axis and the *y*-axis, respectively. Referring to Figure 4, the theoretical dry edge that represents the water stress condition is defined along the edge that connects the *no evaporation* and the *no transpiration* points. While the theoretical wet edge, which represents the well-watered condition, is defined by the horizontal line that connects the *maximum evaporation* and the *maximum transpiration* points. In Figure 4, values along the Ts axis reflect the effects of water content and topography over the bare lands, while values along the VIs axis show the effects of the water content and vegetation density over the vegetative land. The values inside the trapezoidal shape represent varying vegetation cover between the bare lands and dense vegetation. Note that the trapezoidal shape might be affected by many factors including, (i) evaporation levels; (ii) vegetation density and moisture status; (iii) local climate; (iv) the number of pixels in the scene; and (v) other specific study area characteristics such as topography, soil type, spatial heterogeneity, and latitude. In Figure 4, the dry condition appears in the upper envelope of the trapezoid, A–C, a.k.a "warm edge" whereas the "cold edge" occurs in the lower limit of the trapezoid, B–D. Soil moisture index can be retrieved from the relationship between the LST and NDVI based on the location of a pixel in the LST-NDVI space defined in a scatter plot. Therefore, the soil moisture index ranges between 0 at the "warm edge" and 1 at the "cold edge" (Zhan et al. 2004, Parida et al. 2008). The SMI for a given pixel (LST, NDVI) in the LST-NDVI space can be retrieved as (Sandholt et al. 2002):

$$SMI = \frac{T - T_{min}}{T_{max} - T_{min}} \quad (2)$$

Where T_{max} and T_{min} represents the maximum and minimum slopes of the trapezoid and can be respectively calculated as:

$$T_{max} = a_1 * NDVI + b_1 \quad (3)$$

$$T_{min} = a_2 * NDVI + b_2 \quad (4)$$

where a_1, a_2, and b_1, b_2 are the regression coefficients.

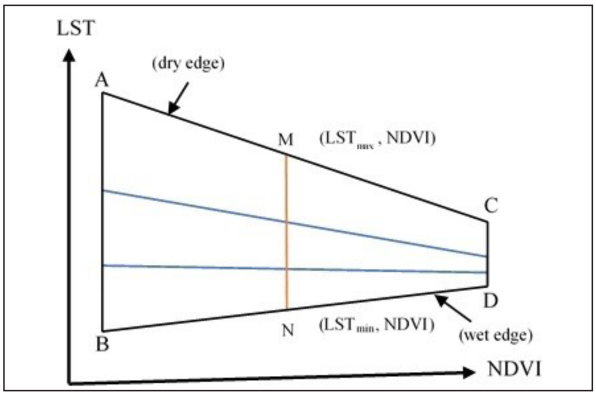

Figure 4. The trapezoidal shape illustrates the relationship between NDVI and LST for estimating soil moisture (after, Zhan et al. 2004)

Data processing

In this study, original NDVI and LST images were used to generate synthetic Landsat-like NDVI and LST by fusing the original MODIS and Landsat 8 using the STI-FM model. The fusion of MODIS and Landsat 8 allows the generation of synthetic images at the spatial resolution of Landsat 8 (i.e., 30m) and the temporal resolution of the MODIS product. From the relationship between the LST and NDVI, the soil moisture index is retrieved.

Statistical analysis

The variation of soil water content in both spatial and temporal scales was determined using statistical analysis such as the spatial and temporal mean, standard deviation, and variation coefficient. The spatial and temporal mean of soil moisture can be respectively calculated as follows (Brocca et al. 2010):

$$\bar{\theta}_j = \frac{1}{N}\sum_{i=1}^{N} \theta_{ij} \quad (5)$$

$$\bar{\theta}_i = \frac{1}{M}\sum_{j=1}^{M} \theta_{ij} \quad (6)$$

Where θ_{ij} is the soil moisture in location (point) *i* and sampling day *j*, *N*, and *M* are the number of measured points and sampling days, respectively? The coefficient of variation *C.V* for both spatial ($C.V_i$) and temporal ($C.V_j$) can be calculated respectively as (Brocca et al. 2010):

$$C.V_i = \frac{\sigma_i}{\bar{\theta}_i} = \frac{\sqrt{\frac{1}{N-1}\sum_{i=1}^{M}(\theta_{ij} - \bar{\theta}_i)^2}}{\bar{\theta}_i} \quad (7)$$

Where σ_i and σ_j are the standard deviation of the spatial and temporal soil moisture?

$$C.V_j = \frac{\sigma_j}{\bar{\theta}_j} = \frac{\sqrt{\frac{1}{N-1}\sum_{j=1}^{N}(\theta_{ij} - \bar{\theta}_j)^2}}{\bar{\theta}_j} \quad (8)$$

The temporal persistence of soil moisture, relative to point *i* and time *j*, is given by (Brocca et al. 2010)

The mean relative difference (MRD) and its standard deviation (SDRD) over the sampling time can be computed as:

$$\delta_{ij} = \frac{\theta_{ij} - \bar{\theta}_j}{\bar{\theta}_j} \quad (9)$$

$$\bar{\delta}_i = \frac{1}{M}\sum_{i=1}^{M} \delta_{ij} \quad (10)$$

$$\sigma_i(\delta_i) = \sqrt{\frac{1}{M-1}\sum_{i=1}^{M}(\delta_{ij} - \bar{\delta}_i)^2} \quad (11)$$

The relationship between the SMI and observed soil moisture from *in-situ* measurements was computed using simple regression analysis. Then, the coefficient of determination (R^2) and the root of mean squared error (RMSE) were used as evaluation metrics of the results using the following equation:

$$r^2 = \left[\frac{\sum(A_{(t)} - \overline{A_{(t)}})(S_{(t)} - \overline{S_{(t)}})}{\sqrt{\sum(A_{(t)} - \overline{A_{(t)}})^2}\sqrt{\sum(S_{(t)} - \overline{S_{(t)}})^2}}\right]^2 \quad (12)$$

$$RMSE = \frac{\sqrt{\sum S_{(t)} - A_{(t)})^2}}{N} \quad (13)$$

Where $A_{(t)}$ and $S_{(t)}$ are the actual and the synthetic Landsat-8 surface reflectance images $A_{(t)}$ and $S_{(t)}$ are the mean values of the actual and the synthetic Landsat-8 images, and *N* is the number of observations.

Geostatistical analysis

To demonstrate the Spatiotemporal pattern of the observed and estimated soil moisture, a geostatistical interpolation technique based on the Ordinary Kriging- semi-variogram function is used. The semi-variogram provides a basic tool for examining spatial autocorrelation as a function of the distance between observations (Romshoo 2004). Generally, the theoretical semi-variogram consists of different models namely linear, spherical, circular, exponential, and Gaussian. The mathematical expression to estimate the semi-variance is defined as (Olea 1999; Webster 2001):

$$\gamma(x) = \frac{1}{2n_h}\sum_{i=1}^{n_h}[z(x_i + h) - z(x_i)h]^2 \quad (14)$$

where $y(x)$ is the empirical semi-variogram; $z(x_i + h)$, $z(x_i)$ is the soil moisture values at sample points x_i *and* $x_i + h$, spaced apart at distance *h*; n_h is the number of pairs $(x_i, x_i + h)$

of soil moisture values at points spaced at distance, used for calculating the semi-variogram function.

Normally, the experimental semi-variogram consists of a nugget, sill, and range. The nugget values do not approach zero at the origin y-axis due to the spatially uncorrelated noise or error in observations, (Kitanidis 1997). The range is a distance where the semi-variogram model first flattens out whereas the sill is a value that the semi-variogram model attains at the range.

The most suitable semi-variogram model is the one that achieves the smallest RMS error between the semi-variance values obtained from the observed soil data and the theoretical model that predicts the semi-variance values. Following published research (e.g., Romshoo 2004; Kumar et al. 2014), the spherical model has been found the best model that achieves the smallest RMSE between the actual and theoretical model computed semi-variance values. Thus, this study employed the spherical semi-variogram model for determining the spatiotemporal pattern of soil moisture. The spherical semi-variance models can be given as (Kumar *et al.* 2016, Romshoo 2004)

$$\gamma(x) = \begin{cases} 0, & h = 0 \\ C_0 + C\left(\frac{3}{2}\frac{h}{a} - \frac{1}{2}\frac{h^3}{a^3}\right) & 0 < h \le a \\ C_0 + c & h > a \end{cases} \quad \text{......................} \ (15)$$

The parameters, C_0 and a denote nugget and effective range respectively, $C_0 + C$ is the sill, and C is the partial sill.

3. Results and discussion

NDVI-LST space for retrieving SMI

The NDVI-LST space using synthetic images derived from the STI-FM data fusion algorithm was used for retrieving monthly surface soil moisture for the growing season from November 2019 to May 2020 in the study area. The computed SMI reflects the vegetation and temperature conditions in the study area. From Figure 5, the NDVI-LST space showed trapezoidal shapes. As such increase in NDVI values reflects a decrease in the LST values and vice versa. As shown in Figure 5, the relationship between the NDVI-LST is clear in wet and cold months (November to March). On the contrary, the situation is different in the warm months (April and May) as an increase in LST joined with an increase in NDVI in the study area. This situation can be seen when comparing the trapezoidal shapes in these months. This can be related to the increase in LST which in turn causes an increase in evapotranspiration and hence a reduction of soil water content and vegetation cover. As a result, the retrieved SMI based on the relationship between the NDVI and LST reflects a realistic soil water content during the wet and cold months compared with those of the warm and dry months.

Figure 6 shows the spatial distribution of SMI in the study area during the study period. It showed the regions which exhibit a high level of soil moisture in five categories with equal interval breaks to emphasize the amount of soil moisture values relative to other values. Generally, the eastern part of the study area showed the lowest values of soil moisture while the central and western areas exhibit the highest. This might be due to (i) the variation in climate conditions as the eastern part observes higher temperatures and lower precipitation values than those for the western parts, (ii) soil properties which consisted of a higher percentage of sand in the eastern part compared to clay, silt, and loam in the central and western parts (see Figure 3). As a result, the SMI in the eastern part does not exceed 0.4 while it reaches more than 0.6 in the central and western parts in almost all the months of the study period. It can also be seen that the topography condition plays another crucial role in determining the SMI values in the study area. This predominantly occurs when comparing the SMI in the central part with those in the western part. Since the central part is almost a plain area that includes a clay texture and deep soil layer, the SMI was always larger than 0.4. On the other hand, the complex relief, mixed soil texture, mixed natural vegetation (e.g., evergreen oak and pine), and shallow soil layer controlled the SMI values in the western part.

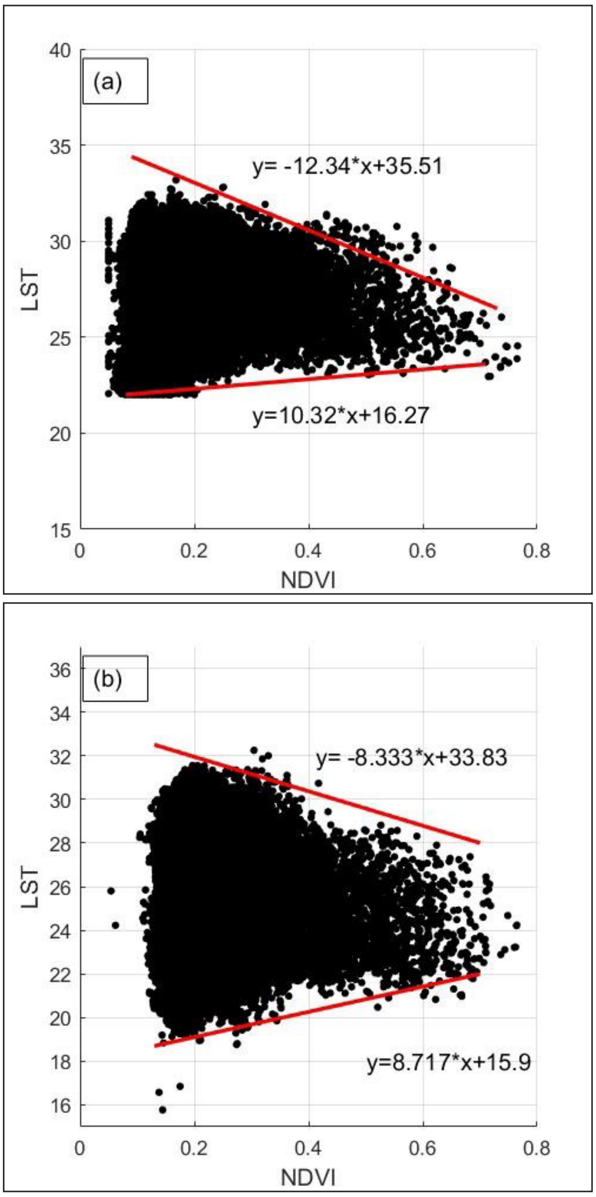

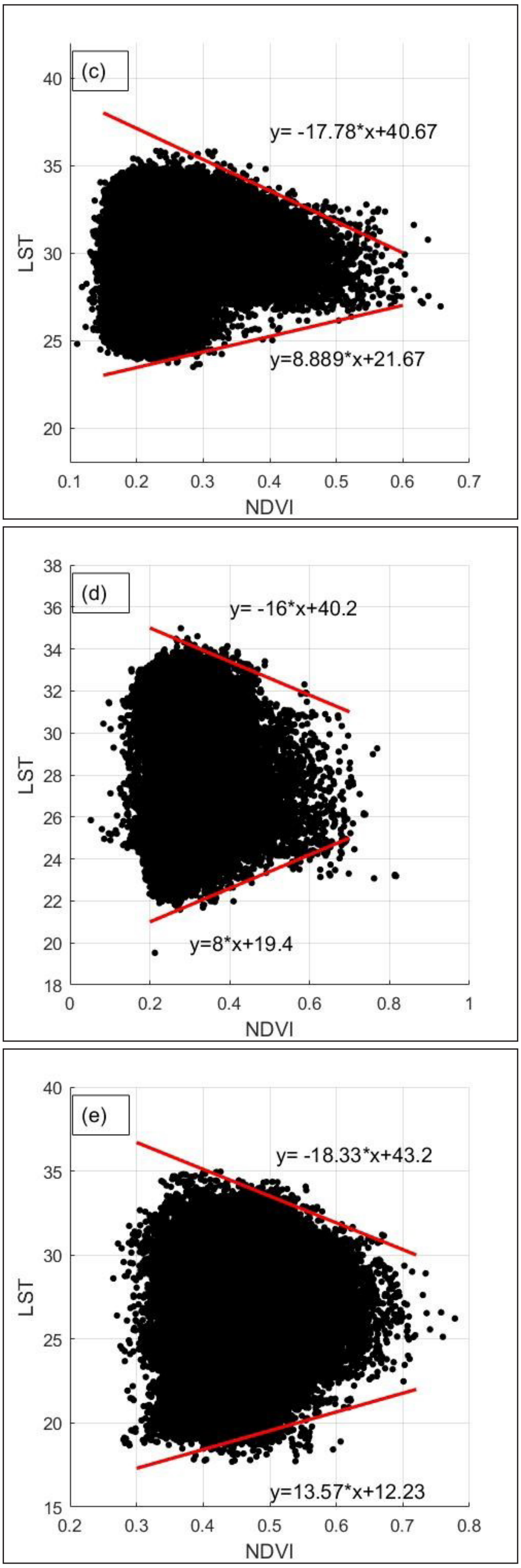

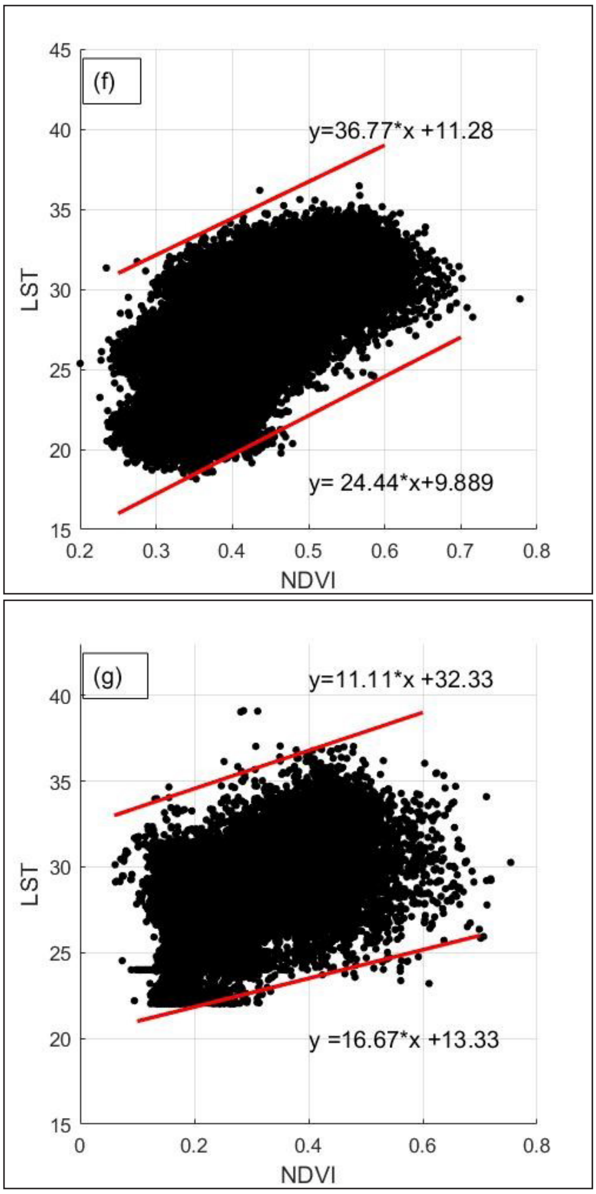

Figure 5. NDVI-LST space for (a) November, (b) December, (c) January, (d) February (e) March (f) April, and (g) May with maximum and minimum slope lines and regression coefficients

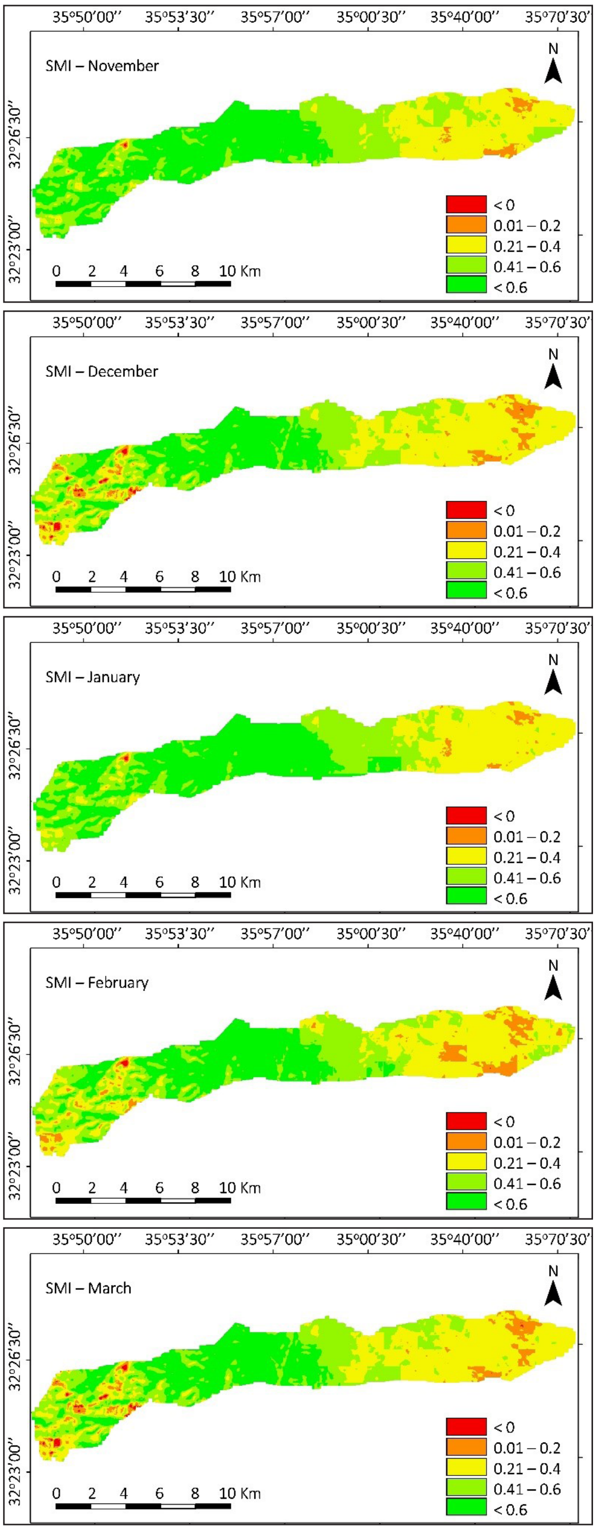

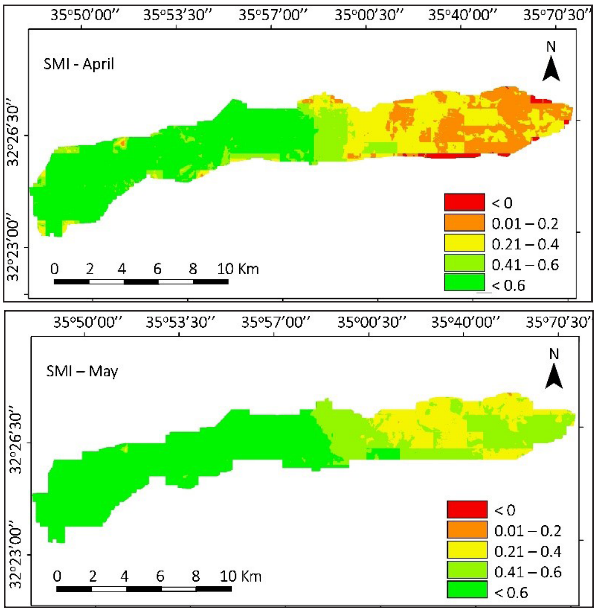

Figure 6. The spatial distribution of soil moisture index (SMI) during the study period from November 2019 to May 2020 in the study area

Soil moisture index and its validation

In this study, 16 *in-situ* measurements were used to validate the estimated SMI from synthetic Landsat 8 images. Figure 7 illustrates the relationship between the measured and estimated SMI along with the quantitative results of the determination coefficient (R^2) and root mean square error (*RMSE*). In general, the trend of the distribution of points was closely distributed to the regression line, this means that the estimated SMI results were close to the soil moisture *in-situ* measurements. Moreover, a moderate correlation between the estimated SMI and the *in-situ* measurements is obvious in the study area during the wet months such as 0.66, 0.62, and 0.49 in January, February, and April. Whereas weak correlation values were observed during November (0.38), December (0.38), and May (0.35). These results indicated that the value of SMI increases in wetter months (i.e., January and February) and decreases in lower precipitation (i.e., November and December) and warmer months (i.e., May). This means that a high amount of rainfall leads to an increase in the soil water content and hence enriches the vegetation cover. The RMSE values, on the other hand, ranged between 0.10 in January to 0.32 in May and thus it behaves oppositely with r^2 and confirmed its results.

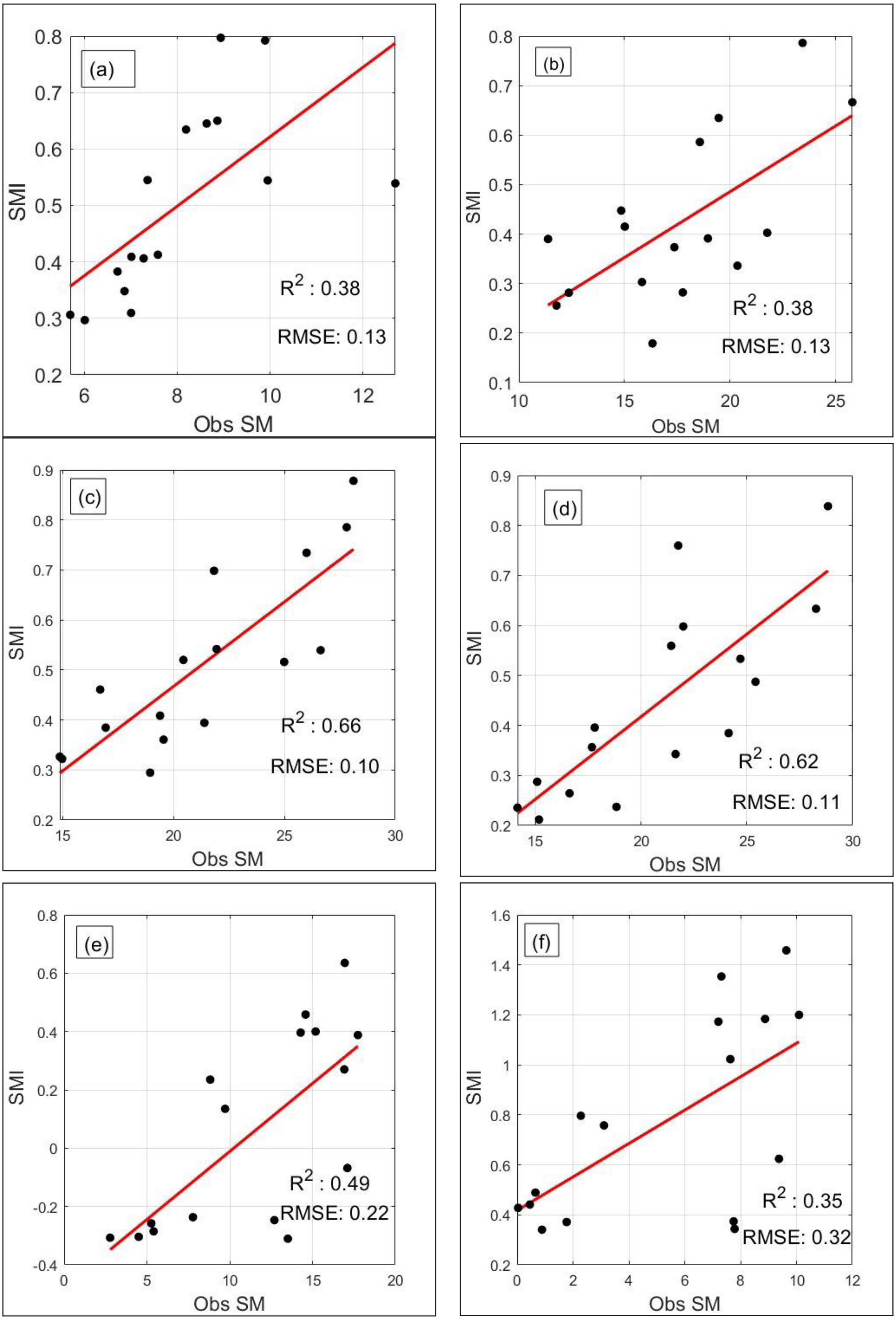

Figure 7. Relationship between observed soil moisture and estimated soil moisture index (SMI) in (a) November, (b) December, (c) January, (d) February, (e) April, and (f) May. Note that the in-situ measurements of soil moisture for March were not performed due to the Covid-19 lockdown restrictions in the study area.

Statistical analysis of the observed soil moisture and SMI

The variation of the soil moisture index, as well as observed soil moisture in both spatial and temporal dimensions, is statistically presented to illustrate whether both the SMI and observed soil moisture vary in a similar pattern. This includes spatial and temporal averages, standard deviation, variation coefficient, mean relative difference and root mean square error (RMSE). Figure 8 shows the temporal averages, the standard deviation, and the variation coefficient of the observed soil moisture and SMI of the 16 *in-situ* measurements. The temporal average in both the observed soil moisture and SMI was similar. This means that when the temporal average of observed soil moisture for a measurement point is high, it is also high for that point in the case of SMI and vice versa. For instance, the average in sample points 3-9 fluctuates between 9– 12% and 0.2-0.3 in the observed soil moisture and SMI, respectively. In both observed soil moisture and SMI, the average in these points was relatively less than the other data sample points. For the other sample points (10-16) the average ranges between 15 -20% in the case of the observed soil moisture, and thus it coincides with those in the SMI. The fluctuations of the temporal averages are attributed to the different climate conditions, topography, soil texture, and vegetation cover in the study area. The standard deviation reflects the temporal variations of soil moisture in the study area as such a huge change in soil water content of a point reflects a large standard deviation and vice versa. Overall, the standard deviation was relatively low in both observed soil moisture and SMI. In the case of the observed soil moisture, the variation coefficient showed that sample points 1-9 have high variations because their values range between 75-38% whereas the rest sample points have a steady stable variation with values ranging between 40-45%. For the SMI variation coefficient, the values were relatively high (around 100%) for sample points 3-9 while it was between 40-60% for the other sample points.

For the spatial analysis, the average, standard deviation, and variation coefficient for the observed soil moisture and the SMI are presented in Figure 9. The spatial average increases with the increase in rainfall and vice versa. Thus, for the observed soil moisture case, the highest spatial averages occurred in January and February during the study period. In these months, the spatial averages were 20% whereas the averages in November, December, April, and May were approximately 9, 17, 11, and 5%, respectively. For the SMI case, the averages ranged between 0.4 and 0.5 from November to the end of February, then it rapidly fell to approximately 0.1 in April and ended up at 0.7 in May. Since the relationship between the NDVI and LST controls the SMI, the growing season, which starts in November and extends until May, reflects an increase in SMI. In April, the evapotranspiration exceeds the precipitation, and therefore, the decay of vegetation causes a reduction of SMI. Notably, the high values of SMI in May are attributed to the vegetative propagation of the natural vegetation (e.g., pine, oak, and wild pistachios) and orchards (e.g., apricot, nectarine, and nuts). Since the variation of the spatial average in the observed soil moisture and SMI is relatively small, the standard deviation and variation coefficient values were steadily stable throughout the whole study period.

The results of temporal stability analysis including the mean relative difference (MRD), the RMSE, and standard deviation for the observed soil moisture and the SMI are depicted in Figure 10. The purpose of MRD is to compare the soil moisture value at a particular data point to the average over the study area. Thus, a point is deemed to be dry or moist if it is less or greater than zero, respectively. To determine whether the soil moisture in a point is in stable status or not, the standard deviation of mean relative difference (SDRD) is normally used. As such low SDRD represents temporal stability whereas a large SDRD indicates that the soil moisture in a point is not linearly related to the study area.

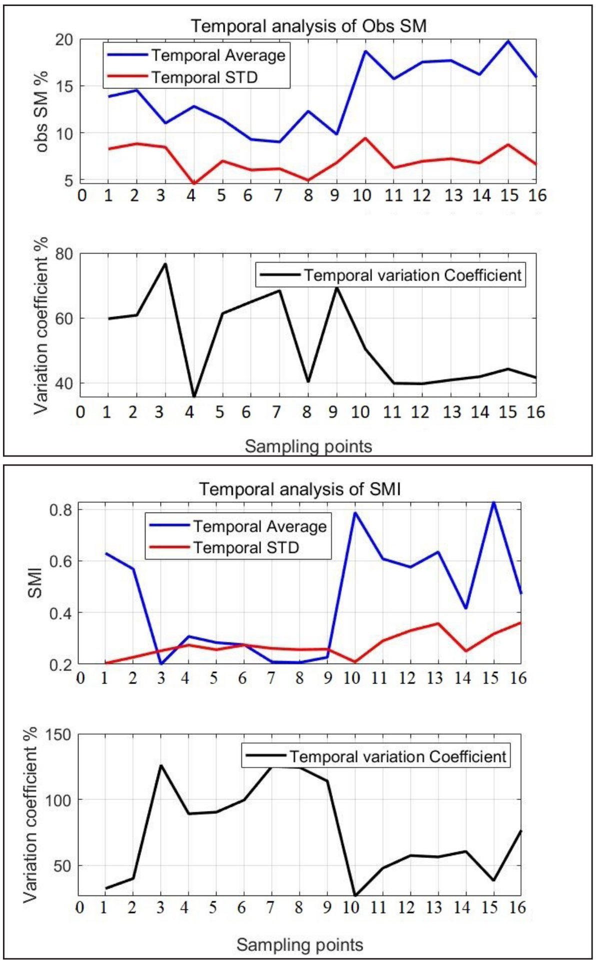

Figure 8. Temporal average, standard deviation, and variation coefficient for the observed soil moisture (up) and SMI (bottom)

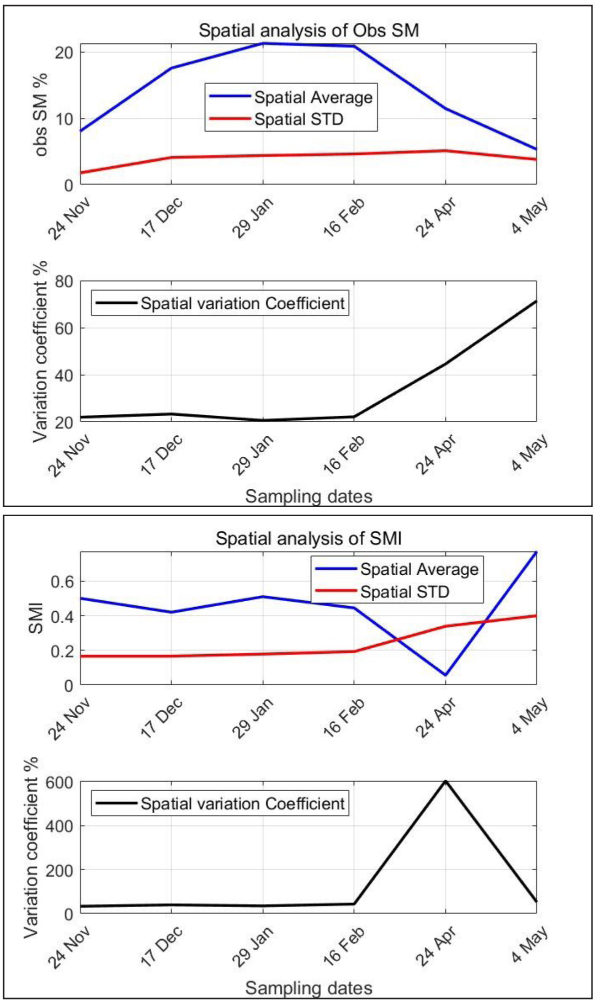

Figure 9. Spatial average, standard deviation, and variation coefficient for the observed soil moisture (up) and SMI (bottom)

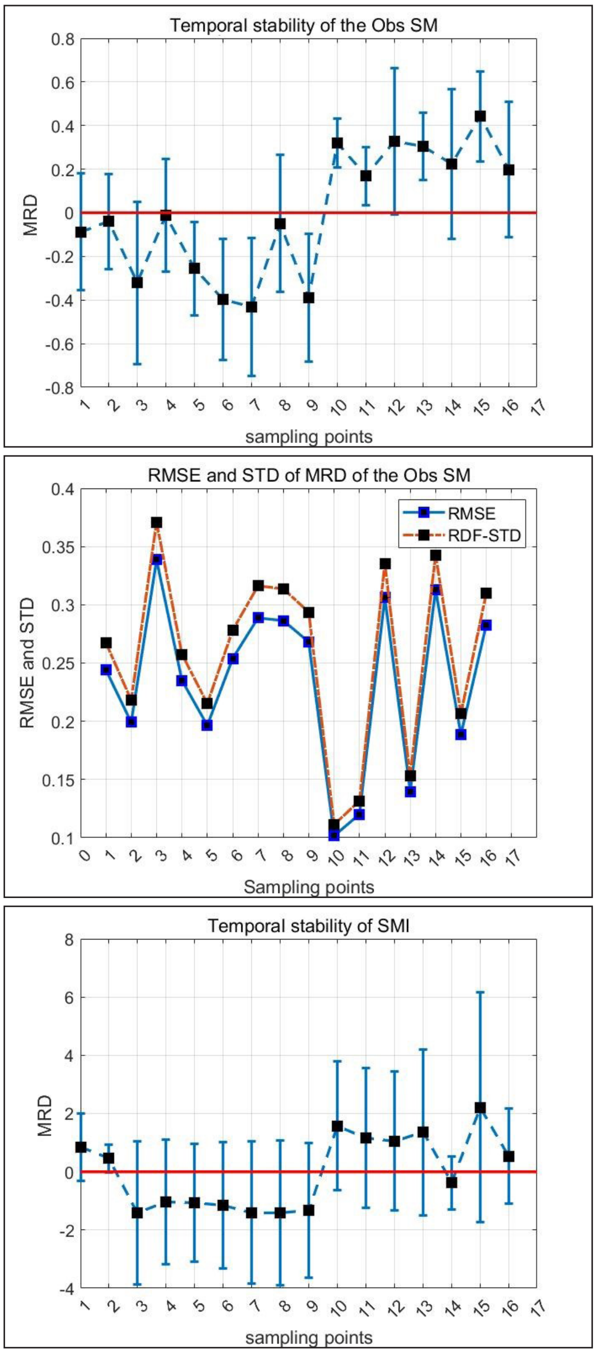

In the case of the observed soil moisture, two groups can be found in terms of dry and moist status. The first group is dry and includes sample points 1-9 as their MRD values were below the mean (zero). The second group, on the other hand, consisted of sample points 10-16 which were found as moist samples as their MRD values were above the mean. This might be related to the location of the first group which represents a semi-arid area whereas the second group belongs to a sub-humid area. For the SMI, the situation was slightly different because sample points 3-9 and sample point number 14 had MRD values below the mean, while the rest of the data points had MRD values greater than the mean.

A clear image can be observed when comparing the values of SDRD and RMSE for each data point for both observed and SMI. For the observed soil moisture, the highest SDRD values (above 0.3%) were found for sample points 3, 7, 8, 12, 14, and 15, whereas the lowest SDRD values (0.15%) were noticed in points 10, 11, and 13. This means that the points which have low SDRD values were temporarily stable while the other data points exhibited large variations within a short time. In the case of the SMI, the opposite situation can be noticed for points 14 and 15 because their SDRD and RMSE values were different from those obtained by the observed soil moisture. Therefore, these data points were not linearly linked to the observed soil moisture.

Spatiotemporal variability of soil moisture

Figure 11 shows the semi-variogram analysis of the 16 soil moisture locations over the whole study period. This is to clarify the spatial autocorrelation among soil moisture observations as a function of distance. As can be seen in Table 3, the minimum and maximum nugget values of 1.11 and 6.42 occur in November and April respectively. Since the nugget values were relatively high in some months, some factors other than the distance between observations influence soil moisture variability. The lowest sill values occur in the driest periods (November, April, and May) with values varying from 0.61 to 7.59. On the other hand, the sill values in December, January, and February (wet periods) are 18.30, 28.54, and 32.7 respectively. The range of correlation length varies from 10545 m in April to approximately 29428 m from November to February.

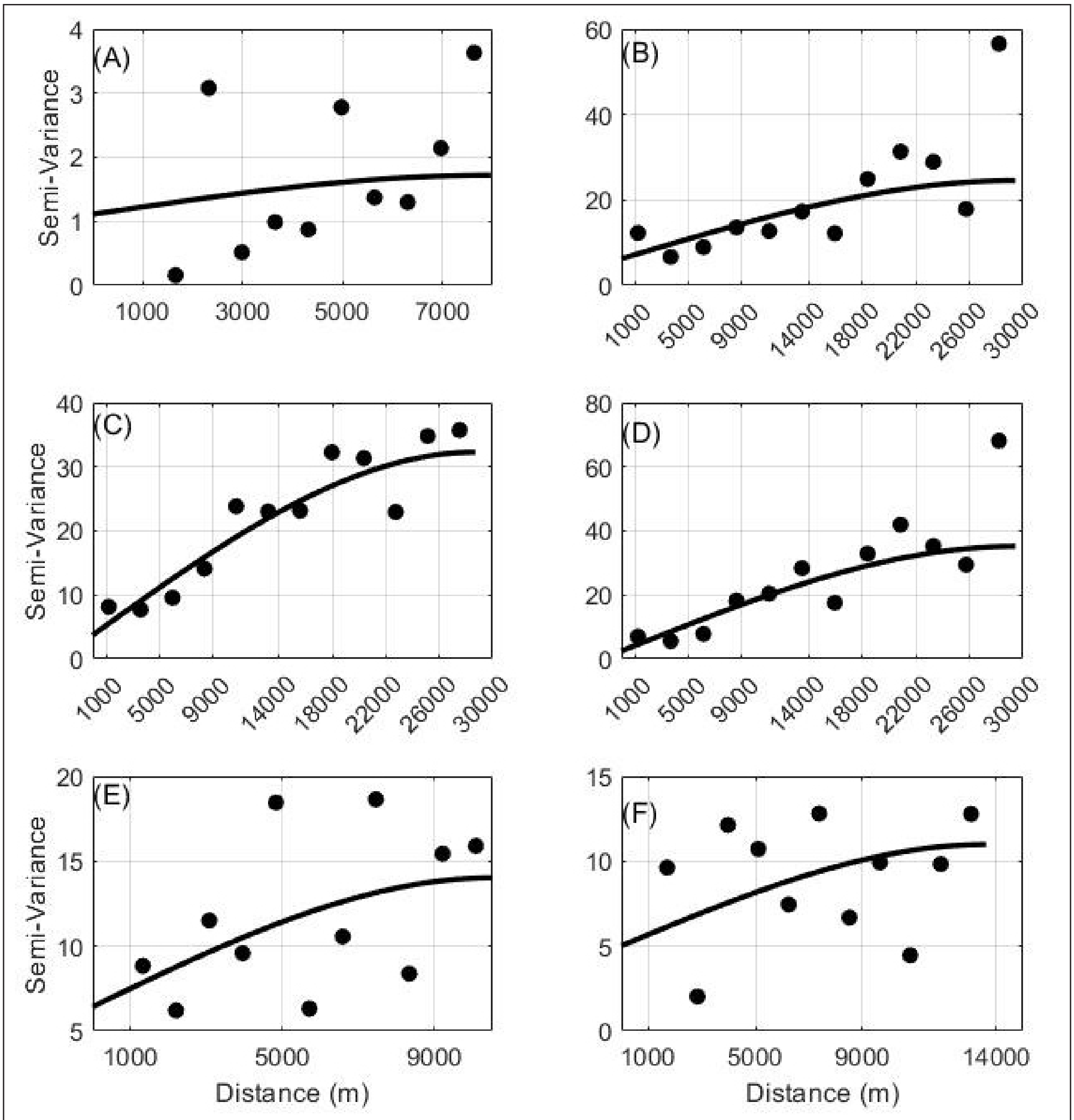

Figure 11. Semi-variogram analysis of the observed soil moisture in (A) November, (B) December, (C) January, (D) February, (E) April, and (F) May. The black dots represent the soil observations.

Table 3. Semi-variogram model elements (range, sill, and nugget) of the observed soil moisture samples over the study period (24th November 2020 to 15th May 2021)

date of sample observation	Nugget	Sill	Range (m)
24-Nov 2020	1.11	0.610	29428
17-Dec 2020	6.26	18.30	29428
29-Jan 2021	3.74	28.54	28718
18-Feb 2021	2.47	32.70	29428
24-Apr 2021	6.42	7.59	10545
15-May 2021	5.02	5.96	13630

For the case of SMI, the Analysis of the Spherical semi-variogram model is depicted in Figure 12 and Table 4. Throughout the study period, the nugget values varied from 0.001 to 0.009 and this reflects a tiny error in soil moisture observations. The sill values are opposite to those found in the case of observed soil moisture because the lowest values were observed during the wet period (December, January, and February) whereas the drier period, such as April and May, in particular, exhibit higher values. This reflects a larger correlation length (range) in the drier period and a shorter range during the wet period.

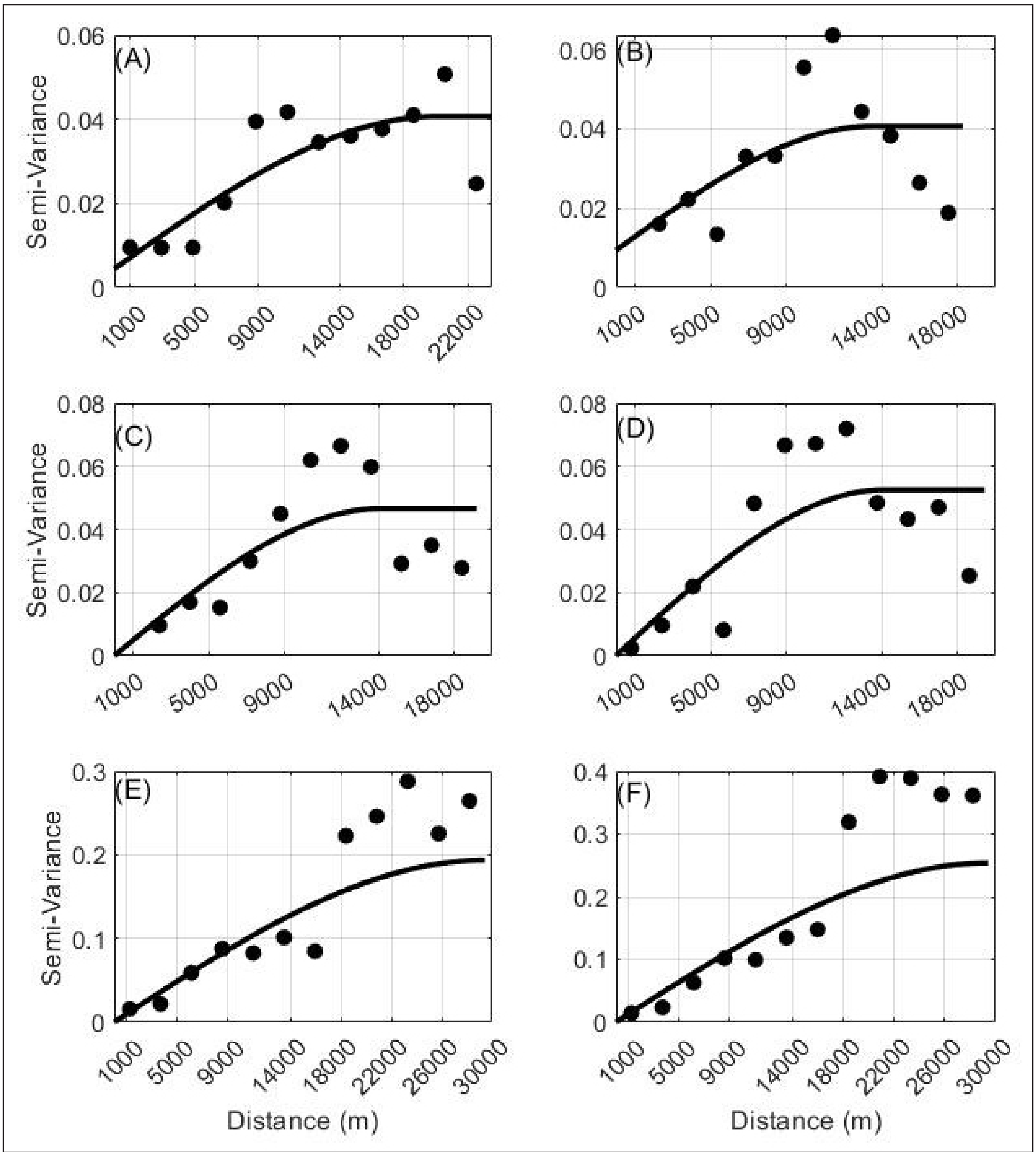

Figure 12. Semi-variogram analysis of SMI in (A) November, (B) December, (C) January, (D) February, (E) April, and (F) May. The black dots represent the soil observations.

Table 4. Semi-variogram model elements (range, sill, and nugget) of SMI over the study period (24th November 2020 to 15th May 2021)

date of images	nugget	sill	range
24-Nov	0.004	0.036268	20125
17-Dec	0.009	0.031228	13544
29-Jan	0.001	0.046645	14149
18-Feb	0.001	0.052551	14139
24-Apr	0.001	0.19372	29428
15-May	0.001	0.25382	29428

4. Conclusions

High spatial and temporal resolutions make satellite images valuable resources for soil moisture monitoring when the ground-based measurements are absent or not evenly distributed. However, due to the trade-off between spatial and temporal resolution of satellite data and the possibility of cloud contamination, new spatiotemporal data fusion techniques were developed and used to generate synthetic satellite-like images. In this context, STI-FM was used to generate synthetic NDVI and LST by fusing MODIS and Landsat 8 products. The correlation between the NDVI and LST images was tested and used to calculate the SMI over a heterogenous study area in northern Jordan during the growing season from November 2019 to May 2020. Results showed that the NDVI-LST relationship is an objective and robust metric for estimating and identifying the spatial distribution of soil moisture in the study area. The results also show a moderate correlation between the measured and SMI for the wetter months and a low correlation in the drier months. The high correspondence between SMI calculated based on the NDVI-LST relationship and independent in-situ metrics demonstrates the high potential of satellite images in monitoring and identifying the spatial distribution of soil moisture in the study area. Furthermore, the results of the semi-variogram analysis for the observed soil moisture show that the drier months have higher soil moisture variability than the wet months. For the case of SMI, the semi-variogram analysis showed no seasonal pattern of soil moisture variability. It was demonstrated that the NDVI-LST relationship and SMI are likely linked to a different climate, soil, and terrain properties in the study area which has a strong impact on spatiotemporal variability/stability of soil moisture.

References

Adegoke, J. O., and Carleton A. M. 2002. Relations between soil moisture and satellite vegetation indices in the US corn belt, J. Hydrometeorol., 3(4), 395– 405. doi:10.1175/1525-7541(2002)003<0395: RBSMAS>2.0.CO;2.

Almagbile, A., Zeitoun, M., Hazaymeh, K., Sammour, H., and Sababha, N. 2019. "Statistical analysis of estimated and observed soil moisture in sub-humid climate in north-western Jordan." Environ Monit Assess 191, 96. doi:10.1007/s10661-019-7230-9.

Beven, K., and Kirkby, M. 1979. "A physically based, variable contributing area model of basin hydrology." Hydrological Sciences Bulletin 24(1), 43-69. DOI: 10.1080/02626667909491834.

Bogena, H. R., Huisman, J. A., Oberdörster, C., and Vereecken, H. 2007. "Evaluation of a low-cost soil water content sensor for wireless network applications." Journal of Hydrology 344, 32–42. DOI: 10.1016/j.jhydrol.2007.06.032.

Brocca, L., Melone, F., Moramarco, T., and Morbidelli, R. 2010. "Spatial-temporal variability of soil moisture and its estimation across scales." Water Resources Research 46, 1-14. DOI: 10.1029/2009WR008016.

Carlson, T.N. 1986. "Regional-scale estimates of surface moisture availability and thermal inertia using remote thermal measurements." Remote Sens. Rev 1 (2), 197–247. DOI: 10.1080/02757258609532069.

Carlson, T. 2007. "An Overview of the "Triangle Method" for Estimating Surface Evapotranspiration and Soil Moisture from Satellite Imagery." Sensors 7: 1612–1629. doi:10.3390/s7081612.

Choi, M., and Y. Hur. 2012. "A Microwave-Optical/Infrared Disaggregation for Improving Spatial Representation of Soil Moisture Using AMSR-E and MODIS Products." Remote Sensing of Environment 124: 259–269. doi:10.1016/j.rse.2012.05.009.

Dorigo, W. A., Wagner, W., Hohensinn, R., Hahn, S., Paulik, C., Drusch, M., Mecklenburg, S., van Oevelen, P., Robock, A., and Jackson, T. 2011. "The International Soil Moisture Network: a data hosting facility for global in situ soil moisture measurements." Hydrology and Earth System Sciences 15, 1675–1698. doi.org/10.5194/hess-15-1675-2011.

Fan, L., Al-Yaari, A., Frappart, F., Swenson, J.J., Xiao, Q., Wen, J., Jin, R., Kang, J., Li, X., and Fernandez-Moran, R. 2019. "Mapping Soil Moisture at a High Resolution over Mountainous Regions by Integrating with Situ Measurements, Topography Data, and Modis Land Surface Temperatures." Remote Sens 11(6), 656. DOI: doi.org/10.3390/rs11060656.

Farrar, T. J., Nicholson, S. E., and Lare, A. R. 1994. "The influences of soil type on the relationships between NDVI, rainfall, and soil moisture in semiarid Botswana. II. NDVI response to soil moisture." Remote Sensing of Environment 50 (2), 121–133. DOI: 10.1016/0034-4257(94)90039-6.

Gao, F., Masek, J., Schwaller, M., and Hall, F. 2006. "On the blending of the Landsat and MODIS surface reflectance: predicting daily Landsat surface reflectance." IEEE Trans. Geosci. Remote Sens 44, 2207–2218. DOI: 10.1109/TGRS.2006.872081.

Gillies, R.R., and Carlson, T.N. 1995. "Thermal remote sensing of surface soil water content with partial vegetation cover for incorporation into climate models." J. Appl. Meteorol 34 (4), 745–756. doi: 10.1175/1520-0450(1995)034<0745: TRSOSS>2.0.CO;2.

Grabs, T., Seibert, J., Bishop, K., Laudon, H. 2009. "Modeling spatial patterns of saturated areas: a comparison of the topographic wetness index and a dynamic distributed model." J. Hydrol 373, 15–23. DOI: 10.1016/j.jhydrol.2009.03.031.

Hazaymeh K., and Almagbile A. 2018. "A comparative analysis of spatiotemporal data fusion models for Landsat and modis data." Int. Arch. Photogramm. Remote Sens. Spatial Inf. Sci., XLII-3,", 7–10 May, Beijing, China. 491–495, doi:10.5194/isprs-archives-XLII-3-491-2018.

Hawley, M.E., Jackson, T.J. & McCuen, R.H. 1983. "Surface soil moisture on small agricultural watersheds". Journal of Hydrology, 62: 179–200.

Hazaymeh, K., and Hassan, Q.K. 2015a. "Spatiotemporal image-fusion model for enhancing the temporal resolution of Landsat-8 surface reflectance images using MODIS images." J. Appl. Remote Sens 9, 96095. DOI: 10.1117/1.JRS.9.096095.

Hazaymeh, K., and Hassan, Q.K. 2015b. "Fusion of MODIS and Landsat-8 Surface Temperature Images: A New Approach." PLoS One 10, 117755. DOI: 10.1371/journal.pone.011775.

Hills, T.C., and Reynolds, S.G. 1969. "Illustrations of soil moisture variability in selected areas and plots of different sizes." Journal of hydrology 8 (1), 27-47. DOI: 10.1016/0022-1694(69)90029-8.

Ibrahim M., Koch B., and Datta P. 2021. Evaluate the effect of land surface temperature in arid and semi-arid lands using potential remote sensing data and GIS techniques. International Journal of Global Warming. 24: 342-355.

Jaber S.M. 2021. "On the relationship between normalized difference vegetation index and land surface temperature: MODIS-based analysis in a semi-arid to the arid environment." Geocarto International. 36: 1117-1135.

Jaber S.M. 2018. "Landsat-based vegetation abundance and surface temperature for surface urban heat island studies: the tale of Greater Amman Municipality." Annals of GIS. 24: 195-208.

Kitanidis, P.K. 1997. "Introduction to Geostatistics: Application to Hydrogeology." University Press, Cambridge.

Kumar, K.; Arora, M.K.; Hariprasad, K.S. 2016. Geostatistical analysis of soil moisture distribution in a part of Solani river catchment. Appl. Water Sci., 6, 25–34.

Jin, T. T., Fu, B. J., Liu, G. H., and Wang, Z. 2011. "Hydrologic feasibility of artificial forestation in the semi-arid Loess Plateau of China." Hydrol. Earth Syst. Sci. 15(8), 2519–2530. DOI: 10.5194/hess-15-2519-2011.

Liu W. T., and Kogan, F. N. 1996. "Monitoring regional drought using the Vegetation Condition Index." International Journal of Remote Sensing 17 (14), 2761-2782, DOI: 10.1080/01431169608949106.

Mohanty, B. P., Skaggs, T. H., and Famiglietti J. S. 2000. "Analysis and mapping of field-scale soil moisture variability using high-resolution, ground-based data during the Southern Great Plains 1997 (SGP97) Hydrology Experiment." Water Resour. Res 36, 1023– 1031, doi:10.1029/1999WR900360.

Mohanty, B. P., Skaggs, T. H. 2001. "Spatial-temporal evolution and time stable characteristics of soil moisture within remote sensing footprints with varying soil, slope and vegetation. Advances in Water Resources, 24, 1051-1067.

Olea R.A. 1999. "Geostatistics for engineers and earth scientists." Boston. Springer. ISBN 978-0-7923-8523-3 pp. 303.

Parida, B. R., Collado, W. B., Borah, R., Hazarika, M. K., and Samarakoon, L. 2008. "Detecting Drought-Prone Areas of Rice Agriculture Using a MODIS-Derived Soil Moisture Index." GIScience & Remote Sensing 45(1), 109-129, DOI: 10.2747/1548-1603.45.1.109.

Qiu Y., Fu B, Wang J, and Chen L. 2001. "Soil moisture variation in relation to topography and land use in a hillslope catchment of the Loess Plateau, China." Journal of Hydrology 240, 243–263. doi:10.1016/S0022-1694(00)00362-0.

Robinson, D. A., Campbell, C. S., Hopmans, J. W., Hornbuckle, B. K., Jones, S. B., Knight, R., Ogden, F., Selker, J., and Wendroth, O. 2008. "Soil moisture measurements for ecological and hydrological watershed scale observatories: a .org/10.2136/vzj2007.0143.

Robock, A., Vinnikov, K.Y., Srinivasan, G., Entin, J.K., Hollinger, S.E., Speranskaya, N.A., Liu, S., and Namkhai, A. 2000. "The global soil moisture data bank." Bulletin of the American Meteorological Society 81, 1281–1299. DOI: 10.1175/1520-0477(2000)081<1281:TGSMDB>2.3.CO;2.

Romshoo, S. A. 2004. "Geostatistical analysis of soil moisture measurements and remotely sensed data at different spatial scales." Environmental Geology, volume 45, pages339–349.

Sandholt, I., Rasmussen, K., and Anderson, J. 2002. "A simple interpretation of the surface temperature/vegetation index space for assessment of the surface moisture status." Remote Sensing of Environment 79: 213–224. doi:10.1016/S0034-4257(01)00274-7.

Schnur, M.T., Xie, H., and Wang, X. 2010. "Estimating root zone soil moisture at distant sites using MODIS NDVI and EVI in a semi-arid region of southwestern USA".

Sun, L., and Sun, R. 2012. "Monitoring surface soil moisture status based on remotely sensed surface temperature and vegetation index information." Agric. For. Meteor 166–167, 175–187. doi: 10.1016/j.agrformet.2012.07.015.

Seneviratne, S. I., Corti, T., Davin, E. L., Hirschi, M., Jaeger, E. B., Lehner, I., Orlowsky, B., and Teuling, A. J. 2010. "Investigating soil moisture-climate interactions in a changing climate: a review." Earth-Science Reviews 99(3–4), 125–161. doi.org/10.1016/j.earscirev.2010.02.004.

Wang, X., Xie, H., Guan, H., and Zhou, X. 2007. "Different responses of MODIS-derived NDVI to root-zone soil moisture in semi-arid and humid regions." J. Hydrol. 340 (1–2), 12–24. doi.org/10.1016/j.jhydrol.2007.03.022.

Webster, R. M. 2001. "Geostatistics for environmental scientists." Chichester. John Wiley and Sons. ISBN 0471965537 pp. 271.

Weng, Q., Fu, P., and Gao, F. 2014. "Generating daily land surface temperature at Landsat resolution by fusing Landsat and MODIS data." Remote Sens. Environ 145, 55–67. doi.org/10.1016/j.rse.2014.02.003.

Western, A. W., and Blöschl, G. 1999. "On the spatial scaling of soil moisture." J. Hydrol. 217. 203– 224, doi:10.1016/S0022-1694(98)00232-7.

Xu, C, Qu, J., Hao, X., Cosh, M., Prueger, J., Zhu, Z., and Gutenberg, L. 2018. "Downscaling of Surface Soil Moisture Retrieval by Combining MODIS/Landsat and In Situ Measurements. Remote Sens 10, 210. doi.org/10.3390/rs10020210.

Zhan, Z, Qin, Q, and X. Wang, 2004. The Application of LST/NDVI Index for Monitoring Land Surface Moisture in Semiarid Area, Geoscience and Remote Sensing, 2004, IGARSS '04. Proceedings 2004 IEEE International, 3:1551–1555.

Zhang, J., and Oxley, R.R.B. 1994. "A comparison of three methods of multivariate analysis of upland grasslands in North Wales." Journal of Vegetation Science 5(1), 71–76. DOI: 10.2307/3235640.

Zhong, A., Wang, A., Li, J., Xu, T., Meng, D., Ke, Y., Li, X., and Chen, Y. 2018. "Downscaling of passive microwave soil moisture retrievals based on spectral analysis." International Journal of Remote Sensing 39(1), 50-67, DOI: 10.1080/01431161.2017.1378456.